

VLBI Observations of the Gravitational Lens System 0957+561

To appear in the Astronomical Journal, 1995.12.

Submitted 1995.07.06, accepted 1995.08.17.

R. M. Campbell¹, J. Lehar,

Center for Astrophysics, 60 Garden Street, Cambridge, MA 02138

Electronic mail: {rcampbell, jlehar}@cfa.harvard.edu

B. E. Corey,

Haystack Observatory, Off Route 40, Westford, MA 01866

Electronic mail: bec@wells.haystack.edu

I. I. Shapiro, and E. E. Falco

Center for Astrophysics, 60 Garden Street, Cambridge, MA 02138

Electronic mail: {ishapiro, falco}@cfa.harvard.edu

ABSTRACT

We present hybrid maps of the A and B images of 0957+561 from each of four sessions of 6 cm VLBI observations that span the six-year interval 1987–1993. The inner- and outer-jets are clearly detected and confirm the structures reported previously. There is no evidence of change in the separation between the core and inner-jet components, so the prospect of measuring the time delay using differential proper motions is not promising. The flux density in the core of each image peaked between 1989 and 1992. From the variation in these flux densities, we obtain a time-delay estimate of ~ 1 yr.

¹present address: Ionospheric Effects Division, Geophysics Directorate, Phillips Laboratories, Hanscom AFB, MA 01731

1. Introduction

The first gravitational lens system to be discovered, 0957+561 (Walsh, Carswell, & Weymann 1979), remains the most extensively studied and discussed. A major cause of this attention is the prospect of obtaining an estimate of H_0 directly from a cosmologically distant source, bypassing the many calibration-sensitive rungs of the “cosmic distance ladder.” To use a gravitational lens system for this purpose, we require a determination of the mass distribution within the lens (*e.g.*, Falco, Gorenstein, & Shapiro 1991) and the “time delay,” $\Delta\tau$, the difference in propagation times from source to observer via two images (Refsdal 1966).

Efforts to determine $\Delta\tau$ have concentrated on examining correlations between the light curves of the A and B images (in the sense that $\Delta\tau > 0$ implies that image A precedes image B). However, different investigators have obtained different results. Optical light-curves have yielded $\Delta\tau \approx 1.0$ yr (Schild & Thomson 1995 and references therein; Vanderriest *et al.* 1989), while the VLA light-curves have yielded $\Delta\tau \approx 1.5$ yr (Lehár *et al.* 1992). This discrepancy led to the reanalysis of various portions of these data (Press, Rybicki, & Hewitt 1992; Pelt *et al.* 1994; Thomson & Schild 1995). These studies illustrate the difficulties in interpreting the light-curve data.

Campbell *et al.* (1994, hereafter C94) discussed two sessions of 6 cm VLBI observations. Their primary intent was to detect proper motion between the core and inner-jet components of each image. Such proper motion would provide an estimate of $\Delta\tau$, independent of the light-curve analysis. Unfortunately, no significant proper motion was found. Turning instead towards further constraint of the mass distribution within the lens through investigation of gradients in the relative magnification matrix for the two images, we carried out two additional sessions of VLBI observations, separated by the presumed $\Delta\tau$ of 1.5 yr (Press *et al.* 1992). Save for any effects of microlensing, comparison of the two images at the same “source epoch” would isolate the lensing distortions from any intrinsic quasar variability, and thereby provide better constraints on the mass distribution.

2. Observations

We have made simultaneous 6 cm observations of the A and B images of 0957+561 in four sessions (see Table 1). C94 describe results from the first two sessions more fully. The 0957+561 images were observed in 12 minute scans at intervals of about 30 minutes. A few

compact sources were also observed during each session to aid fringe finding. The reference frequency was 4.983 GHz and the recorded bandwidth B was 56 MHz, except at the VLA where $B = 48$ MHz as limited by the front-end filter. We relied on radiometry information supplied by each station to provide the initial flux-density calibration.

For the first two observing sessions (1987 and 1989), each station used the Mk III recording format (Rogers *et al.* 1983) in mode A (14 independent video channels). In the third session (1992), we incorporated some of the new VLBA antennas near the VLA to provide more short baselines. However, the Los Alamos station produced no useful data, due to an equipment failure. Whenever they participated, VLBA stations used the Mk III recording format in mode B (7 video channels, $B = 28$ MHz). This resulted in a $\sim 30\%$ loss in sensitivity for baselines involving at least one of those stations. There were further sensitivity losses in the fourth session (1993): the Hancock VLBA station was substituted for the more sensitive Haystack antenna, and, more significantly, the VLA replaced their Mk III acquisition system with a VLBA acquisition rack, resulting in a similar bandwidth reduction.

Data tapes were correlated on the Mk III A processor at Haystack Observatory. Specific correlation procedures are discussed in C94. Baselines involving only a single antenna at each station were correlated twice, once for the coordinates of each image. The VLA and Westerbork could not observe both images simultaneously, so these stations observed each image on alternate scans. Baselines formed exclusively from the set of stations comprising L, K, O, and VLBA antennas (see Table 1 for identifications) were not sensitive enough to detect the images. Detections of the B image on baselines such as G–VLBA were marginal. Following data export from the Haystack correlator, we used the Caltech VLBI Software Package (Pearson 1991) to perform all editing and calibration.

3. Hybrid Maps

We produced hybrid maps of 0957+561 using the DIFMAP software in the Caltech VLBI package (Shepard, Pearson, & Taylor 1994). We initially calibrated the station phases to a point source model, with a flux density of 10 mJy for the A image and 7 mJy for the B image. Eight cycles of CLEAN mapping and self-calibration then followed. In each cycle, we started with a new set of CLEAN components, and broke the CLEANing into four runs, increasing the number of iterations in each successive run. For the first two cycles, we used a small CLEAN window which enclosed only the core and the inner-jet components. In the next two cycles, we included a second window which covered the brightest part of

the outer-jet (Jet 2 in Gorenstein *et al.* 1988). In the third set of two cycles, we used six windows to cover the entire VLBI structure of each image. In the final two cycles, we used the GSCALE routine, which adjusts each station gain by a constant factor to improve the fit of the CLEAN model to the visibilities.

Using this procedure, we produced maps for all four sessions; Table 2 shows some of the results. The self-calibration procedure evaluates closure phases for each individual scan, so those visibilities whose baselines did not form part of a closure triangle at a given time were deleted. The residual map *rms* values were ~ 0.04 mJy/beam for all sets of observations except those from 1993 (our least sensitive array, see §2 above), where the *rms* values were ~ 0.06 mJy/beam. Table 2 lists for each observing session the reduced chi-square, which DIFMAP computes by comparing the observed visibilities to those predicted from the CLEAN model. We have integrated the flux density in a window which encloses only the core and inner-jet components, and we list these as well in Table 2, with standard errors derived from the map *rms*. We also list the *rms* of the GSCALE corrections, as a conservative estimate of the absolute flux-density calibration. The A and B image GSCALE corrections were consistent to $\sim 4\%$ on average, and their ratio did not differ from zero by more than $\pm 7\%$ in any case.

We show the hybrid maps of the inner regions of each image in Figure 1. All the maps show the same basic structure seen in C94. In particular, there is no clear evidence of any change with time in the separation between the core and inner-jet components for either image. We are thus not likely to measure the time delay from differential proper motions in the near future.

The outer-jet is detected in the data from each of the four sessions, and shows similar structure in each. This structure is less reliably determined for the 1989 and 1993 sessions, however, due to poorer data quality (see §2 above; C94). Figure 2 shows the 1992 hybrid maps, convolved with a circular beam of $\text{FWHM} = 6$ mas to emphasize the more extended outer-jet structure. The outer-jet compares very well with that in the 18 cm maps of Garrett *et al.* (1994), and is consistent with the general morphology of the elliptical Gaussian models used in C94. We will report elsewhere on determining the image magnification gradient from the outer-jet structures.

4. Estimation of the Time Delay

The flux densities in the cores of the A and B images vary, and both show a clear peak between 1990 and 1992 (see Table 2). We can obtain from these flux-density measurements

a crude estimate of $\Delta\tau$ and the ratio R of the magnification of the core of the B image to that of the A image. Although the time sampling is very sparse, we can make this estimate by assuming that the core brightness varies smoothly.

We determined $\Delta\tau$ and R simultaneously by fitting a polynomial to the combined A image and (shifted) B image light curves (*e.g.*, Lehár *et al.* 1992). Using our core flux-densities (Table 2), we considered a two-dimensional grid of shifts, covering $-1.5 \text{ yr} < \Delta\tau < 3.5 \text{ yr}$ and $0.4 < R < 0.9$. For each grid point, we obtained a least-squares polynomial fit to the combined light-curves using SVDFIT (Press *et al.* 1989), and the total χ^2 . We set the standard errors of $\Delta\tau$ and R as the range over which $\chi^2 - \chi_{\min}^2 < 1$, where χ_{\min}^2 denotes the minimum value obtained for χ^2 .

Using the map *rms* to set the flux-density errors, we found that a fourth-order polynomial was the lowest order required to model the observed shape of the light-curve, since a third-order polynomial led to a 100-fold increase in χ_{\min}^2 . Thus, with five polynomial parameters, two shift parameters ($\Delta\tau, R$), and eight flux-density constraints, only one degree of freedom remains for each fit. We obtained $\Delta\tau = 0.88 \pm 0.13 \text{ yr}$ and $R = 0.664 \pm 0.007$, with $\chi_{\min}^2 = 0.31$. The upper panel of Figure 3 shows the combined light-curve data with the best-fit polynomial.

A very conservative error estimate is the *rms* of the GSCALE station corrections (see Table 2), because the flux-density calibration is not likely to be wrong by more than the station radiometry errors. Note that radiometry errors for each station are likely to be correlated between sessions. A third-order polynomial suffices to fit the core flux-densities with these errors, giving two degrees of freedom. The resulting time delay and flux-density ratio are $\Delta\tau = 0.5 \pm 0.5 \text{ yr}$ and $R = 0.67 \pm 0.08$, with $\chi_{\min}^2 = 1.86$. The lower panel of Figure 3 shows the corresponding best-fit polynomial. χ_{\min}^2 doubled if we used a second-order polynomial to fit the flux-density variations.

Our image magnification parameter R differs considerably from the core magnification found by other investigators (Conner, Lehár, & Burke 1992, and references therein). However, there are reasons why our result could be in error. Most importantly, the A and B images have different effective baseline sampling, because they are magnified by different factors. The inner-jet of the B image is longer than that of the A image, so some of its flux density may be resolved out by the VLBI sampling. Note also that the B image is dimmer than the A image; the consequently greater number of non-detections of the B image results in a sparser ($u-v$) sampling for it than for the A image, independent of any relative magnification effects.

In any event, the estimated time delay is less sensitive to considerations concerning the

($u-v$) sampling, since $\Delta\tau$ is determined only from the varying portion of the flux density in the core. Given that no structural variations are seen in the inner jet, its brightness is not likely to vary on a timescale of a few years. Thus, any inner-jet flux density which we resolve out in the B image should only affect R and not $\Delta\tau$. Since the flux density of the B image decreased sharply in 1993, our light-curve favors the shorter “optical” delay of ~ 1 yr over the longer “radio” delay of ~ 1.5 yr, but our formal errors are too large to exclude either case. The variation of the flux density in the inner regions of the images from the first two sessions are consistent with the variations observed by the VLA monitoring program (C94, Lehar *et al.* 1992). The subsequent decrease in flux density observed for both images during the last two VLBI sessions should also have been observed with the VLA. Because these latter data contain much more closely spaced samples, and since their calibration should be more reliable, the VLA monitoring program should yield a more precise estimate of $\Delta\tau$ from this feature.

We thank participating observatories and their staffs for supporting our experiments, especially the Haystack correlator staff for ensuring expeditious processing of the 1993 data. Operation of the MkIII correlator at Haystack Observatory was funded by the NSF through the Northeast Radio Observatory Corporation. We acknowledge support from NASA grant NGT-50663 (RMC) and NSF grants AST89-02087 and AST93-03527 (RMC, JL, and IIS).

REFERENCES

- Campbell, R. M., Corey, B. E., Falco, E. E., Shapiro, I. I., Gorenstein, M. V., Elósegui, P., Marcaide, J. M., & Alvi, K. 1994, *ApJ*, 426, 486 (herein C94)
- Conner, S. R., Lehar, J., & Burke, B. F. 1992, *ApJ*, 387, L61
- Falco, E. E., Gorenstein, M. V., & Shapiro, I. I. 1991, *ApJ*, 372, 364
- Garrett, M. A., Calder, R. J., Porcas, R. W., King, L. J., Walsh, D., & Wilkinson, P. N. 1994, *MNRAS*, 270, 457
- Gorenstein, M. V., Cohen, N. L., Shapiro, I. I., Rogers, A. E. E., Bonometti, R. J., Falco, E. E., Bartel, N., & Marcaide, J. M. 1988, *ApJ*, 344, 42
- Lehar, J., Hewitt, J. N., Roberts, D. H., & Burke, B. F. 1992, *ApJ*, 384, 453
- Pearson T. J. 1991, *BAAS*, 23, 991
- Pelt, J., Hoff, W., Kayser, R., Refsdal, S., & Schramm, T. 1994, *A&A*, 286, 775
- Press, W. H., Flannery, B. P., Teukolsky, S. A., & Vetterling, W. T. 1989, *Numerical Recipes* (Cambridge: Cambridge University Press)

- Press, W. H., Rybicki, G. B., & Hewitt, J. N. 1992, ApJ, 385, 416
- Refsdal, S. 1966, MNRAS, 132, 101
- Rogers, A. E. E. *et al.* 1983, Science, 214, 51
- Schild, R., & Thomson D. J. 1995, AJ, 109, 1970
- Shepard, M. C., Pearson, T. J., & Taylor, G. B. 1994, BAAS, 26, 987
- Thomson, D. J., & Schild, R. 1995, in Proceedings of the International Conference on Applications of Time Series Analysis and Meteorology, in press
- Vanderriest, C., Schneider, J., Herpe, G., Chevreton, M., Moles, M., & Wlérick, G. 1989, A&A, 215, 1
- Walsh, D., Carswell, R. F., & Weymann, R. J. 1979, Nature, 279, 381

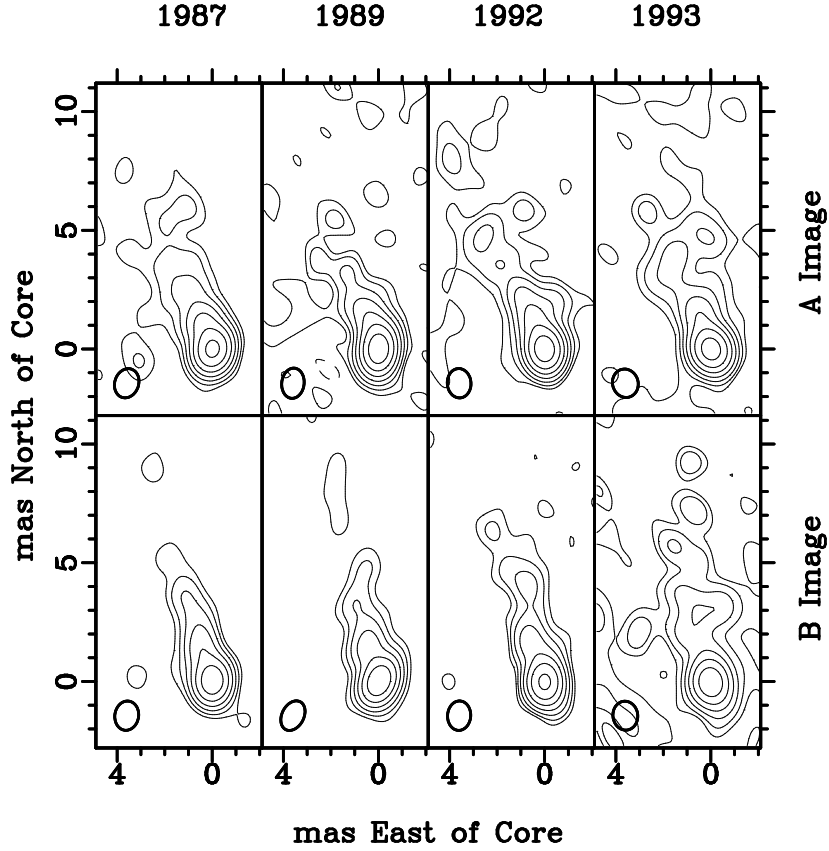


Figure 1: Hybrid maps of the core and inner-jet of 0957+561 A and B, for all four sessions of 6 cm observations. The ~ 1 mas diameter restoring beam is shown as an ellipse in the lower left of each field, and was chosen to represent the angular resolution of each observation, using the “uniform” baseline weighting scheme (Shepard *et al.* 1994). The pixel size is 0.1 mas, and the map contours increase by factors of two from 0.125 mJy/beam to 8 mJy/beam.

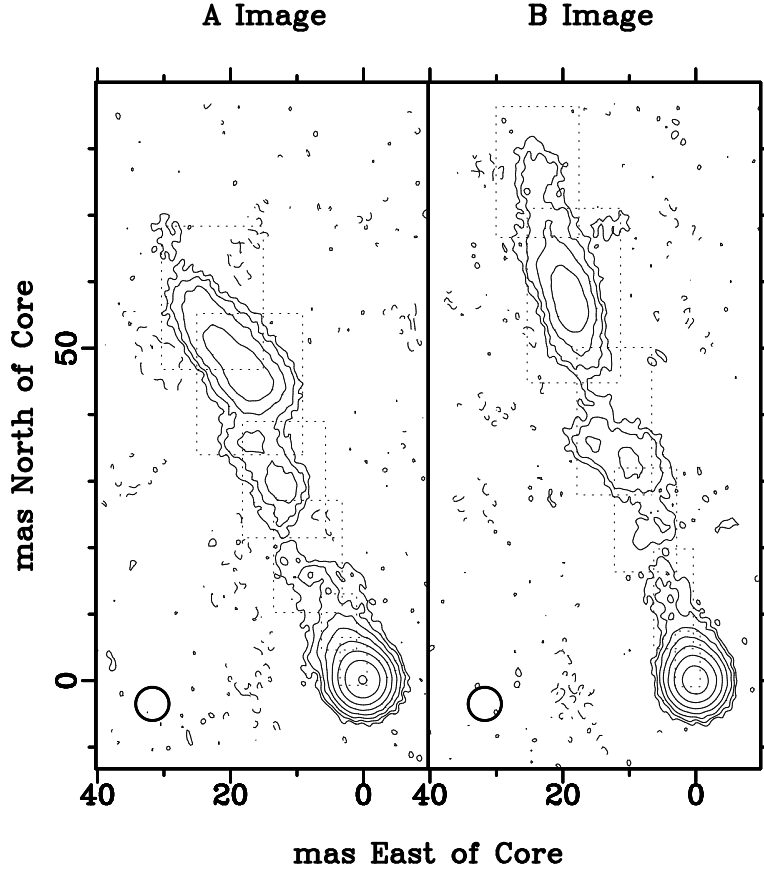


Figure 2: Hybrid maps of 0957+561 A and B, from the 1992 6 cm observations. We convolved the clean components with a circular, $\text{FWHM} = 6 \text{ mas}$ beam to emphasize the outer-jet structure. The six CLEAN windows are outlined with dotted lines, and the restoring beam is shown in the lower left of each field. The pixel size is 0.25 mas , and the map contours increase by factors of two from 0.125 mJy/beam to 16 mJy/beam .

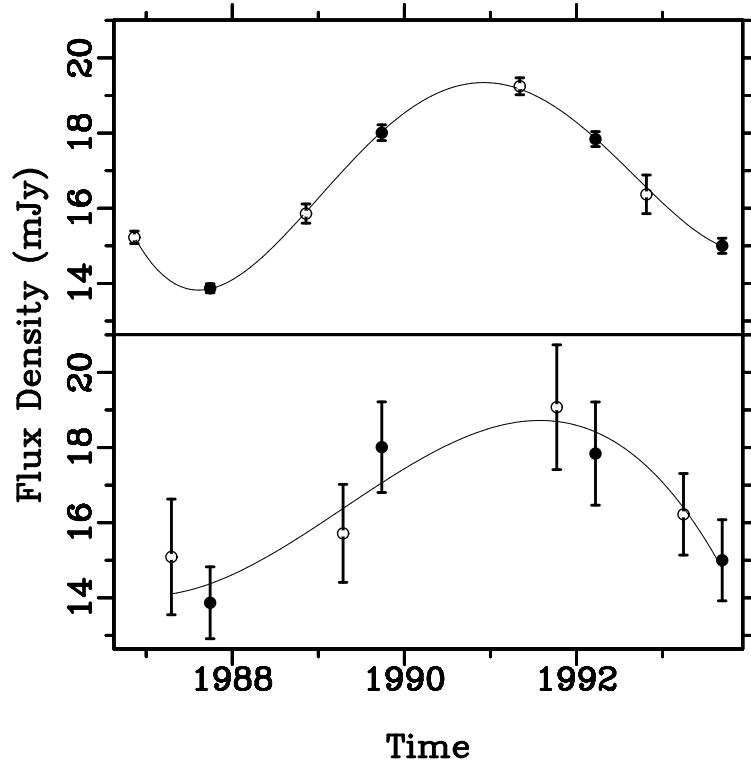


Figure 3: Combined VLBI light curves for the core of 0957+561. The observed A-image flux densities are shown as filled circles. The B-image data have been shifted by the least-square estimates of $\Delta\tau$ and R , and are shown as empty circles. We also show the least-squares polynomial light curves. The upper panel shows the result of analysis using the map *rms* flux-density errors (*i.e.*, we fit a fourth-order polynomial light curve), and the lower panel shows the result of analysis using the GSCALE error estimate (*i.e.*, we fit a third-order polynomial light curve).

Table 1: Summary of Observations

Start Date	Start UT	Duration	#Baselines (Image A,B)	Stations ^{a,b}
1987.09.28	09:30	13 hr	18,12	L–B–W–K–G–Y–O
1989.09.26	09:00	15 hr	14,13	B–W–K–G–Y–O
1992.03.21	21:00	13 hr	15,15	L–B–K–G–Y–Kp–Ov
1993.09.10	09:30	15 hr	17,17	L–B–Hn–G–La–Y–Kp–Ov

^a VLBI Network: B=Bonn, G=Green Bank 43m, K=Haystack,
L=Medicina, O=Owens Valley 40m, W=Westerbork, Y=VLA

^b VLBA Antennas: Hn=Hancock, Kp=Kitt Peak, La=Los Alamos, Ov=Owens Valley

Table 2: Hybrid Mapping Results

Observation Date:Image	#Visibilities Total:Deleted ^a	Core Region Flux Dens. ^b	Scale Error ^c	Reduced χ^2
1987:A	692:48	13.87 ± 0.12	6.9%	0.86
1989:A	534:96	18.01 ± 0.21	6.7%	0.98
1992:A	855:80	17.84 ± 0.20	7.7% ^d	0.93
1993:A	1068:196	15.00 ± 0.20	7.2%	1.13
1987:B	529:145	10.11 ± 0.11	10.2%	0.68
1989:B	411:183	10.53 ± 0.17	8.3%	0.88
1992:B	785:104	12.78 ± 0.15	8.7% ^d	0.93
1993:B	1028:194	10.87 ± 0.34	6.7%	1.48

^a visibilities were deleted if either antenna was not part of any closed loop of baselines

^b in mJy; error from the *rms* of the CLEAN map

^c the *rms* of station gain corrections in GSCALE

^d excludes the VLBA antennas, whose T_{sys} values were $> 20\%$ higher than expected